



# Self-Assembled Monolayers of N-Heterocyclic Olefins on Au(111)

Iris Berg, Luca Schio, Justus Reitz, Elena Molteni, Linoy Lahav, Carolina Gutiérrez Bolaños, Andrea Goldoni, Cesare Grazioli, Guido Fratesi, Max M. Hansmann, Luca Floreano, and Elad Gross\*

**Abstract:** Self-assembled monolayers (SAMs) of N-heterocyclic olefins (NHOs) have been prepared on Au(111) and their thermal stability, adsorption geometry, and molecular order were characterized by X-ray photoelectron spectroscopy, polarized X-ray absorption spectroscopy, scanning tunneling microscopy (STM), and density functional theory (DFT) calculations. The strong  $\sigma$ -bond character of NHO anchoring to Au induced high geometrical flexibility that enabled a flat-lying adsorption geometry via coordination to a gold adatom. The flat-lying adsorption geometry was utilized to further increase the surface interaction of the NHO monolayer by backbone functionalization with methyl groups that induced high thermal stability and a large impact on work-function values, which outperformed that of N-heterocyclic carbenes. STM measurements, supported by DFT modeling, identified that the NHOs were self-assembled in dimers, trimers, and tetramers constructed of two, three, and four complexes of NHO–Au-adatom. This self-assembly pattern was correlated to strong NHO–Au interactions and steric hindrance between adsorbates, demonstrating the crucial influence of the carbon-metal  $\sigma$ -bond on monolayer properties.

## Introduction

The strong affinity of N-heterocyclic carbene (NHC) ligands to metals, metal-oxides, and semimetals enabled the formation of NHC-based self-assembled monolayers (SAMs) on a variety of surfaces.<sup>[1]</sup> The thermal stability<sup>[2]</sup> and synthetic versatility<sup>[3]</sup> of NHCs have made NHC-based SAMs a viable alternative to thiol-based monolayers. Due to these advantages, NHC-based SAMs were applied as (bio)sensors,<sup>[3b,g,k,4]</sup> ligands for nanoparticles and clusters,<sup>[1e,2c,3a,5]</sup> molecular probes for surface reactivity,<sup>[6]</sup>

modifiers for electronic devices,<sup>[3d,7]</sup> corrosion inhibitors,<sup>[8]</sup> and co-catalysts.<sup>[3a,9]</sup>

NHCs are well-established ligands in transition metal chemistry and homogeneous catalysis. While  $\sigma$ -donation is the most important component of metal-ligand binding, NHCs also function as  $\pi$ -accepting ligands.<sup>[10]</sup> Their  $\sigma$ -donor ability makes them suitable surface binders for late-transition metals, such as gold.<sup>[2a,11]</sup> Self-assembly of various classes of NHCs was investigated to identify the influence of the carbene ring properties on surface-anchoring. This includes carbenes such as cyclic (alkyl)(amino)carbenes (CAAC)<sup>[3c,12]</sup> with a single nitrogen atom in the carbene heterocycle, and triazolone-based compounds,<sup>[13]</sup> such as nitron.<sup>[14]</sup> However, in all aforementioned ligands, surface-anchoring was induced via the carbene carbon thus combining both  $\sigma$ -donation and  $\pi$ -back-donation capabilities and restricting the disentangling of these two effects.

N-heterocyclic olefins (NHOs) represent a different class of carbon-based ligands that are formally composed of an alkylidene moiety ( $\text{CH}_2$ ) appended to the NHC (Scheme 1a).<sup>[15–17]</sup> NHOs can be represented by a neutral as well as a zwitterionic mesomeric Lewis structure (Scheme 1a).<sup>[18]</sup> The stabilization of the positive charge by the aromatic imidazolium moiety, makes NHOs highly polarized towards the exocyclic carbon atom thus leading to a strong  $\sigma$ -donor, with negligible  $\pi$ -accepting character. The pronounced difference between these overall donor effects is reflected by the low Tolman electronic parameter (TEP) of NHOs compared to NHCs [TEP (NHO)  $\approx$  2025–2030  $\text{cm}^{-1}$ ; TEP (NHC)  $\approx$  2040–2051  $\text{cm}^{-1}$ ].<sup>[19]</sup> Due to these electronic characteristics, NHOs and their derivatives have found broad application in transition metal- and organo-catalysis,<sup>[20]</sup> main-group,<sup>[21]</sup> and coordination chemistry,<sup>[22]</sup> or polymer chemistry.<sup>[23]</sup> However, the utilization of NHOs as

[\*] I. Berg, L. Lahav, Prof. E. Gross  
 Institute of Chemistry and The Center for Nanoscience and  
 Nanotechnology, The Hebrew University, Jerusalem 91904 (Israel)  
 E-mail: elad.gross@mail.huji.ac.il

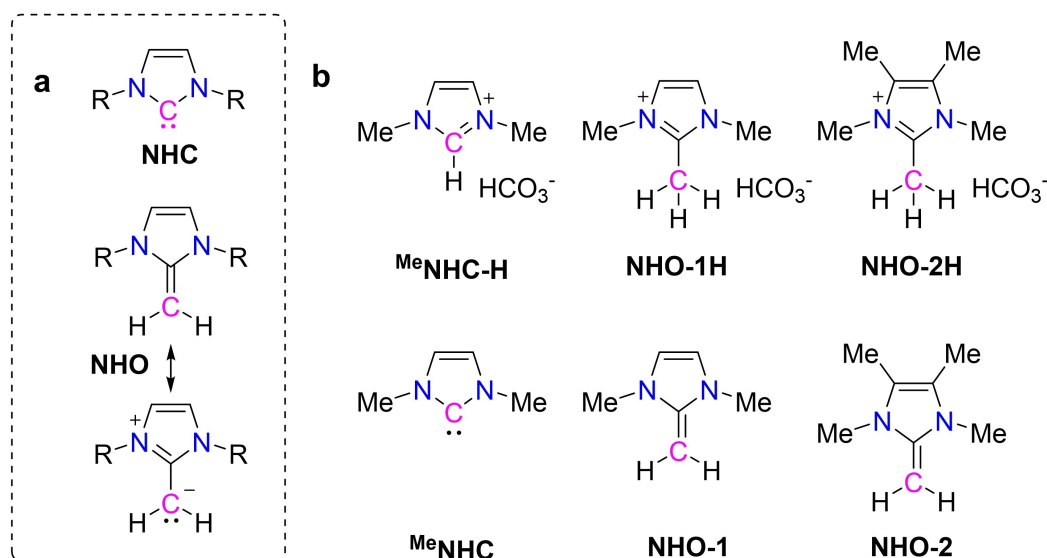
Dr. L. Schio, Dr. C. Grazioli, Dr. L. Floreano  
 CNR-IOM, Laboratorio TASC, Basovizza SS-14, Km 163.5, Trieste  
 34012 (Italy)

J. Reitz, Prof. M. M. Hansmann  
 Technische Universität Dortmund, Fakultät für Chemie und Chemi-  
 sche Biologie, Otto-Hahn-Str. 6, 44227 Dortmund (Germany)

Dr. E. Molteni, Prof. G. Fratesi  
 Dipartimento di Fisica “Aldo Pontremoli” Università degli Studi di  
 Milano, Via Celoria 16, 20133 Milano (Italy)

C. G. Bolaños, Dr. A. Goldoni  
 Elettra-Sincrotrone Trieste S.C.p.A, Basovizza SS-14, Km 163.5,  
 Trieste 34149 (Italy)

© 2023 The Authors. Angewandte Chemie International Edition published by Wiley-VCH GmbH. This is an open access article under the terms of the Creative Commons Attribution Non-Commercial NoDerivs License, which permits use and distribution in any medium, provided the original work is properly cited, the use is non-commercial and no modifications or adaptations are made.



**Scheme 1.** a) Molecular structures of NHCs and NHOs. b) Molecular structures of 1,3-dimethyl imidazolium hydrogen carbonate ( $^{\text{Me}}\text{NHC-H}$ ), 1,2,3-trimethyl imidazolium hydrogen carbonate (NHO-1H), and 1,2,3,4,5-pentamethyl imidazolium hydrogen carbonate (NHO-2H) that were used as precursors for vapor deposition of  $^{\text{Me}}\text{NHC}$ , NHO-1 and NHO-2, respectively, on Au(111).

surface ligands that can decouple the  $\sigma$ -donation and  $\pi$ -back-donation properties was not yet explored.

In this work we show that NHOs derived from their protonated imidazolium salts (NHO-1/2H) (Scheme 1b) are self-assembled on Au(111) via  $\sigma$ -bond interaction with Au-atom, forming a pattern of dimers, trimers and tetramers that are constructed of NHO–Au-atom complexes. The  $\sigma$ -bond character provided geometrical flexibility, enabling a flat-lying adsorption geometry that induced high thermal stability and substantially reduced the substrate work-function. The high flexibility of surface-anchored NHOs enabled to further increase their surface interaction by backbone functionalization that also resulted in an improved thermal stability.

## Results and Discussion

The self-assembly of NHO-1 and NHO-2 on Au(111) were studied and the properties of NHO monolayers were compared to that of  $^{\text{Me}}\text{NHC}$ , which serves based on its structural similarity as a carbene reference to NHO-1 (Scheme 1b). NHO-1 and NHO-2 were chosen for this study to identify the impact of backbone functionalization on NHO self-assembly.<sup>[24]</sup> NHO-1 and NHO-2 are highly air-sensitive compounds, therefore we were interested in air-stable precursors for their in situ generation. In order to find a pathway to generate the desired NHOs on the surface without addition of external base we selected bench-stable hydrogen carbonate salts as precursors, a procedure established for the generation of carbenes on surfaces.<sup>[2b,3b,e,25]</sup> It should be noted that NHO formation and self-assembly can be also achieved by the addition of an external base, which will be described further below.

Based on this procedure,  $^{\text{Me}}\text{NHC}$  as well as NHO-1 and NHO-2 were vapor deposited under ultrahigh vacuum (UHV) conditions on Au(111) while using 1,3-dimethyl imidazolium hydrogen carbonate ( $^{\text{Me}}\text{NHC-H}$ ), 1,2,3-trimethyl imidazolium hydrogen carbonate (NHO-1H) and 1,2,3,4,5-pentamethyl imidazolium hydrogen carbonate (NHO-2H) as precursors for  $^{\text{Me}}\text{NHC}$ , NHO-1, and NHO-2, respectively (for additional synthetic details, see experimental section and Figures S1–S12). Vapor deposition was performed by *in-vacuo* sublimation of the solid precursor at 350 K from a Knudsen cell with a boron nitride crucible.<sup>[3b,e]</sup> The anchoring geometry and thermal stability of the SAMs were characterized using X-ray photoelectron spectroscopy (XPS) and polarized near-edge X-ray absorption fine structure (NEXAFS) measurements (performed at the ALOISA beamline of the ELETTRA synchrotron facility in Trieste, Italy).<sup>[26]</sup>

N1s XPS signals of NHO-1 and NHO-2 on Au(111) were acquired and are shown in Figure 1a and 1b, respectively. XPS measurements were performed following annealing to 150 °C to remove physisorbed residues (Figure S13). The N1s spectra of NHO-1 and NHO-2 was fit to a Gaussian centered at 402.2 and 402.0 eV, respectively (Figure 1a and 1b). A shoulder at lower binding energy was probed for NHO-1 and assigned to physisorbed residues,<sup>[27]</sup> which desorbed upon further annealing. To compare the properties of NHO monolayers with that of NHCs,  $^{\text{Me}}\text{NHC}$  was deposited on Au(111) under UHV conditions and characterized by XPS measurements. The N1s XPS spectrum of  $^{\text{Me}}\text{NHC}$  (Figure 1c) was fit by one main Gaussian that was centered at 401.2 eV, in agreement with previous observations.<sup>[25c]</sup> A minor Gaussian was located at 402.2 eV and assigned to protonated nitrogen.<sup>[28]</sup>

The obtained results demonstrate that NHOs can be self-assembled on Au(111) to form a stable monolayer. The

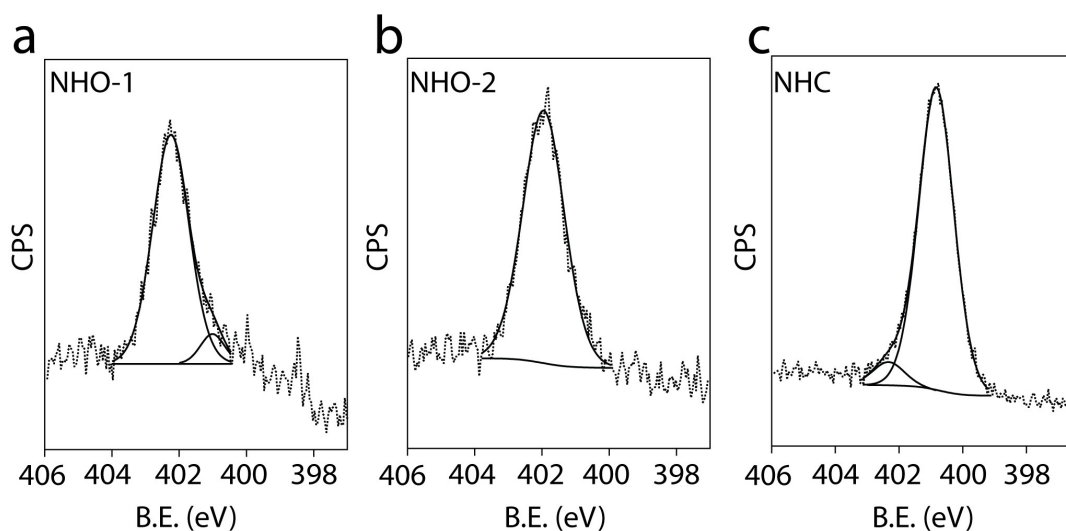


**Figure 1.** N1s XPS signals of (a) NHO-1 (b) NHO-2 and (c) <sup>Me</sup>NHC on Au(111).

N1s XPS signals of the two NHOs were shifted towards higher binding energies than that of <sup>Me</sup>NHC, indicative of a partial positive charge on the nitrogen atoms, which was correlated to the zwitterionic structure of NHO.<sup>[29]</sup> The peak area of NHO-1 and NHO-2 was lower by 53 and 52 %, respectively, than that of <sup>Me</sup>NHC. The lower surface density of NHOs can be linked to their larger molecular footprint and stronger surface interactions, as will be further detailed in STM measurements and DFT calculations.

Nitrogen K-edge NEXAFS measurements were conducted to elucidate the anchoring geometry of NHOs by comparing their p- and s-polarized NEXAFS spectra (marked by solid and dotted lines, respectively, in Figure 2). NEXAFS measurements of NHO-1 and NHO-2 were performed after annealing to 150 and 200 °C, respectively, to remove all physisorbed residues. Nitrogen K-edge NEXAFS spectrum of NHO-1 (Figure 2a) showed a dominant  $\pi^*$  transition at 401.8 eV, correlated to  $N1s \rightarrow \pi^*_{(N=C)}$ ,<sup>[29]</sup> and two

smaller peaks positioned at 398.8 eV and 399.8 eV assigned to  $N1s \rightarrow \pi^*_{(N=C-C)}$  and  $N1s \rightarrow \pi^*_{(N-C-C)}$ , respectively.<sup>[29-30]</sup> Enhanced signal was obtained at p-polarization in the  $\pi^*$  range and implies that the imidazole ring adopted a flat-lying adsorption geometry with respect to the surface normal (see experimental section for details). A continuum of transitions was measured in the  $\sigma^*$  region (404–415 eV), correlated to  $N1s \rightarrow \sigma^*$  transitions.<sup>[29]</sup> In the  $\sigma^*$  region, the intensity of the spectrum at s-polarization was higher than that of p-polarization. The opposite dichroism in the  $\sigma^*$  region is an additional indication for the preference towards a flat-lying orientation with respect to the surface.

Nitrogen K-edge NEXAFS spectra of NHO-2 on Au(111) showed a similar pattern to the one detected for NHO-1 with a dominant  $N1s \rightarrow \pi^*_{(N=C)}$  transition in the  $\pi^*$  region, centered at 401.8 eV, and a clear positive dichroism characteristic of a flat-lying geometry (Figure 2b).  $N1s \rightarrow \sigma^*$  transitions were detected in the  $\sigma^*$  region, and displayed an

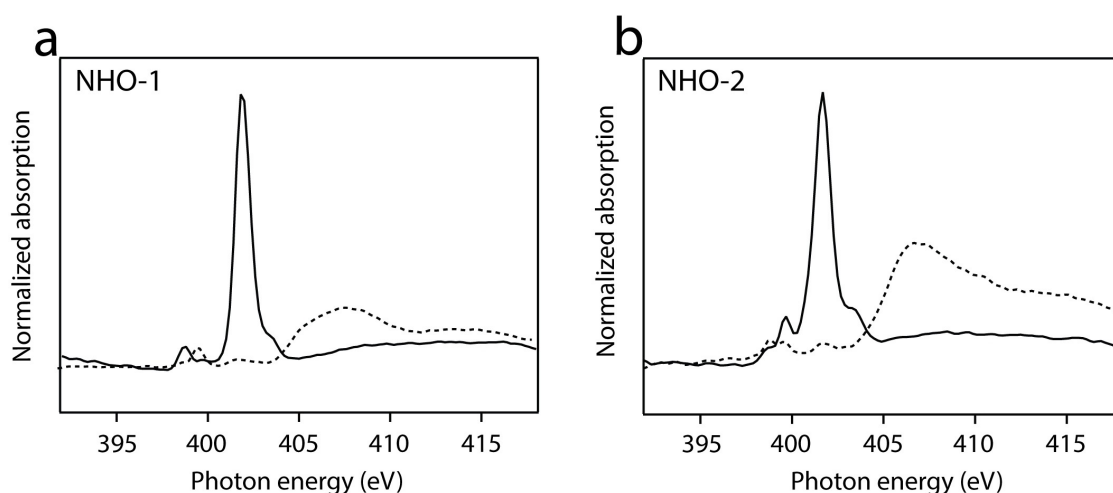


**Figure 2.** Nitrogen K-edge NEXAFS spectra measured at p- and s-polarizations (solid and dotted lines, respectively) of (a) NHO-1 and (b) NHO-2.

opposite dichroism trend comparing to the  $\pi^*$  region, which further specifies that the surface-anchored molecules were adsorbed in a flat-lying geometry. Small transitions were detected at 399.8 and 403.4 eV and correlated to a more oxidized species (Figure 2b).<sup>[3e,31]</sup> Nitrogen and carbon K-edge NEXAFS spectra of <sup>Me</sup>NHC showed similar dichroism, which specified a flat-lying adsorption geometry (Figure S14–S15), in accordance with previous publications.<sup>[11c,25c]</sup>

DFT structural optimizations starting with olefinic (planar) NHO identified an optimal adsorption of NHO-1 (Figure 3a–b) and NHO-2 (Figure 3c–d) on Au(111) and Au-adatoms with a flat-lying adsorption geometry (Table S1). The adsorption energies of NHO-1 and NHO-2 on a Au-adatom were  $-2.73$  and  $-3.00$  eV, respectively, while values lower by  $\sim 0.7$  eV were calculated for NHOs adsorption on Au(111). It should be noted that the energetic stabilization that stems from adsorption on an adatom ( $\Delta E = 0.69$  eV for NHO-2) does not fully compensate for the energetic cost of adatom formation on terrace sites (0.79 eV). Thus, it is hypothesized that NHO-adatom formation was initially induced on step sites, as validated in STM images that showed large meandering and indentation of monoatomic steps following adsorption of NHOs (Figure S16). The adsorption energy of flat-lying <sup>Me</sup>NHC on Au-adatom was  $-2.72$  eV, which is in good agreement with a previous study for NHCs,<sup>[32]</sup> although a larger value was also reported.<sup>[11c]</sup> The calculations hence show that NHO-1 and <sup>Me</sup>NHC have similar adsorption energies, while NHO-2 has a

higher adsorption energy due to backbone functionalization that induced stronger surface interactions.

DFT analysis of bond lengths and bond angles of NHO-1 and NHO-2 was performed to elucidate the ylidic versus olefinic character of surface-anchored NHOs (Scheme 1). The bond length of the carbene carbon with the CH<sub>2</sub> carbon (denoted as C1 and C6, respectively, in Figure S17) was increased by ca. 0.1 Å (NHO-1: 1.364 Å to 1.444 Å; NHO-2: 1.365 Å to 1.447 Å) upon adsorption of both NHO-1 and NHO-2 on a Au-adatom (Table S2). In addition, the calculated bond angle of C1–C6–Au was 107° and 110° for surface-anchored NHO-1 and NHO-2, respectively. Both observations indicate that the CH<sub>2</sub> carbon in surface-anchored NHO is sp<sup>3</sup> hybridized, which is indicative of NHO adsorption in ylidic rather than in olefinic structure. This coordination mode is also in agreement with the homogeneous, molecular Au complexes of NHOs showing an end-on coordination to the metal center with a Au–C bond length of 2.087(3) Å,<sup>[19a]</sup> in a similar range to the calculated values for the Au-surface bound species (2.124 Å to 2.135 Å; Table S2). Analysis of the electron density displacement upon adsorption (Figure S18) highlights an accumulation of charge density between the C6 atom and the Au-adatom with nearly cylindrical symmetry around the Au–C bond, together with a depletion of  $\pi$  charge within the molecule and a minor accumulation of charge in the backbone plane. A strong bonding with the Au-adatom is also recognized by analyzing the electronic density of states projected on atomic orbitals<sup>[33]</sup> showing a large hybridization of the highest occupied molecular orbitals (HOMO) and HOMO-1, both having  $\pi$  symmetry but especially a strong amplitude at the C6 atom, with surface states (Figure S19). These results further rationalize the high adsorption energy of NHOs on Au.

The thermal stabilities of NHO-1, NHO-2 and <sup>Me</sup>NHC were analysed by recording their N1s XPS signal following annealing (Figure 4 and Figure S20). Comparative analysis of the normalized N1s XPS peak area demonstrated the improved thermal stability of NHO-1 and NHO-2 over that of <sup>Me</sup>NHC (Figure 4). The N1s XPS signal of <sup>Me</sup>NHC was reduced by 90% after annealing to 300 °C, while that of NHO-1 and NHO-2 were reduced by 34 and 25%, respectively. NHO-2 showed improved thermal stability, and nitrogen signal was detected even after annealing to 400 °C, and preserved its original peak pattern up to 300 °C (Figure S20). Further annealing of NHO-2 to 350 and 400 °C led to significant peak shifts toward lower binding energies, which may indicate decomposition of the molecules and formation of pyridine species.<sup>[34]</sup> The improved thermal stability of NHO monolayers can be attributed to their strong  $\sigma$  donating properties.<sup>[15]</sup> The enhanced stability of NHO-2, in comparison to NHO-1, is correlated to stronger surface interactions that are induced by the methyl groups on its backbone.

To examine the role of the precursor in NHO self-assembly we also investigated a hydrogen carbonate free synthetic approach and an independent synthetic strategy applying an external base. Self-assembled monolayers of NHO-1 and NHO-2 were prepared by using 1,2,3-trimethyl

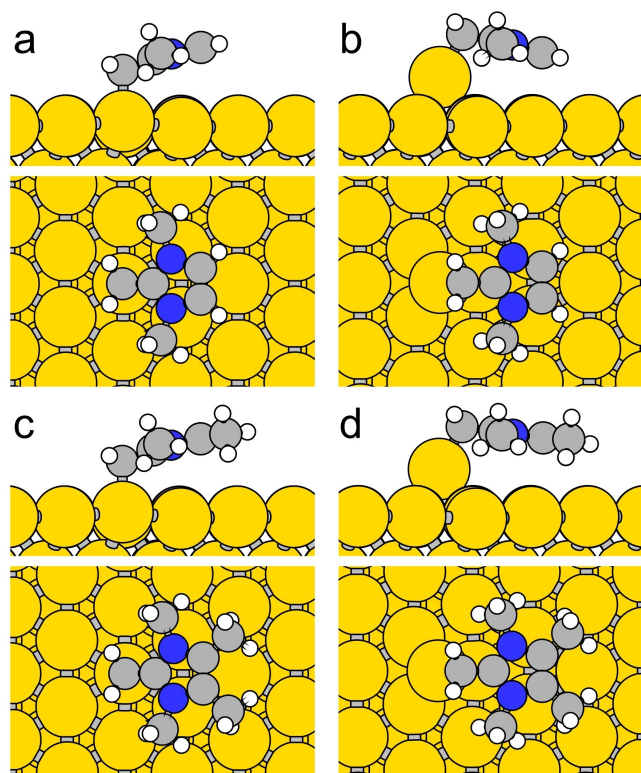


**Figure 3.** Calculated optimized adsorption geometries for NHO-1 (a–b), and NHO-2 (c–d) on a terrace (a, c), and on a Au-adatom (b, d).

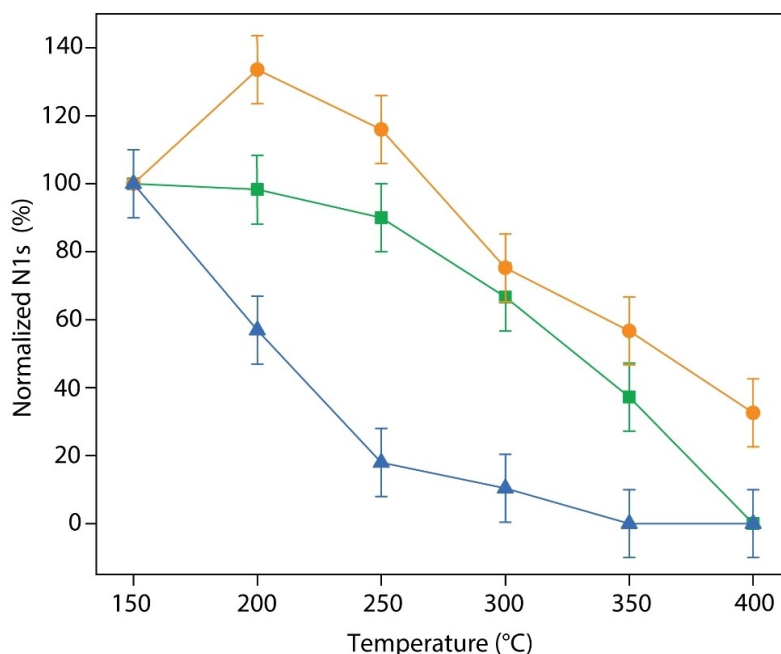


**Figure 4.** Normalized N1s XPS peak area of NHO-1 (green), NHO-2 (orange) and <sup>Me</sup>NHC (blue).

imidazolium and 1,2,3,4,5-pentamethyl imidazolium salts, both containing iodide anions as precursors. Deprotonation was induced by potassium *tert*-butoxide immersed in THF (experimental details are provided in the SI). N1s XPS signal of NHO monolayers that were self-assembled on Au film and prepared while using halide-imidazolium precursors showed an overall similar pattern to that of NHO monolayers prepared via UHV deposition of imidazolium hydrogen carbonate precursors (Figure S22). The N1s/Au4f XPS peak area ratios of NHO-1 and NHO-2, which were prepared by base-induced deprotonation of imidazolium iodide precursors, were comparable to that of NHC monolayers that were prepared by base-induced deprotonation.<sup>[3b,e]</sup>

Deprotonation of 1,2,3,4,5-pentamethyl imidazolium hydrogen carbonate precursor (NHO-2H) for the formation of NHO-2 monolayer was also demonstrated under liquid phase conditions. NHO-2 monolayer was prepared on a Au film, following annealing of THF-solvated NHO-2H at 70 °C. The N1s XPS signal of NHO that was prepared by using solvated 1,2,3,4,5-pentamethyl imidazolium hydrogen carbonate resembled the pattern of the sample prepared by 1,2,3,4,5-pentamethyl imidazolium iodide precursor (Figure S22). These experiments further validate that NHO monolayers can be prepared by using NHO precursors with either halide or hydrogen carbonate anions and deprotonation can be achieved with a strong base or via annealing, respectively.

Slow exchange of the imidazole-CH<sub>3</sub> protons for imidazole-CD<sub>3</sub> was observed in CD<sub>3</sub>CN solution for the hydrogen carbonate salts and indicated the possibility to form the olefin as a transient intermediate (Figure S23 and S24). Heating the hydrogen carbonate precursors NHO-1/2H under vacuum (10<sup>-3</sup> mbar) did not induce sufficient

amounts of NHOs to be detected by NMR, but mostly resulted in sublimation of the salts. These results indicate that mechanistically, deprotonation is either characterized with a very low efficiency (which is sufficient for surface deposition) or that deprotonation is further facilitated by surface interactions.

Low-energy XPS measurements were conducted to quantify the electronic effects of NHO monolayers on the work function of Au(111). Changes in the work function values of  $-1.9 \pm 0.1$ ,  $-2.4 \pm 0.1$  and  $-2.1 \pm 0.1$  V were measured for NHO-1, NHO-2 and <sup>Me</sup>NHC, respectively (Figure S25). These results show that all three molecules significantly reduce the work function of Au, as expected for molecules with high  $\sigma$ -donation affinity and as previously demonstrated for NHC monolayers.<sup>[7a]</sup> NHO-2, which was postulated to be a better  $\sigma$ -donor in comparison to <sup>Me</sup>NHC and NHO-1, induced a noticeable decrease in the work function value that outperformed that of NHCs. It should be noted that the surface density of NHOs was lower by 50% in comparison to that of NHCs. Thus, the normalized effect of NHOs is larger in comparison to NHCs, in line with their strong donor characteristics.

The self-assembly pattern of NHOs on Au(111) was imaged using STM measurements. High mobility of both NHO-1 and NHO-2 was detected, which prevented their high-resolution imaging at room temperature (Figure S16). Low-temperature (130 K) STM imaging of NHO-1 (Figure 5a–c) and NHO-2 (Figure 5d–f) on Au(111) revealed that NHOs were self-assembled in units of trimers and tetramers structures. The average height of isolated NHO-1 and NHO-2 was 105 and 80 pm, respectively, which is indicative of a flat-lying adsorption geometry. For both NHOs, a similar self-assembly pattern was observed, though lower surface density was identified for NHO-1, possibly

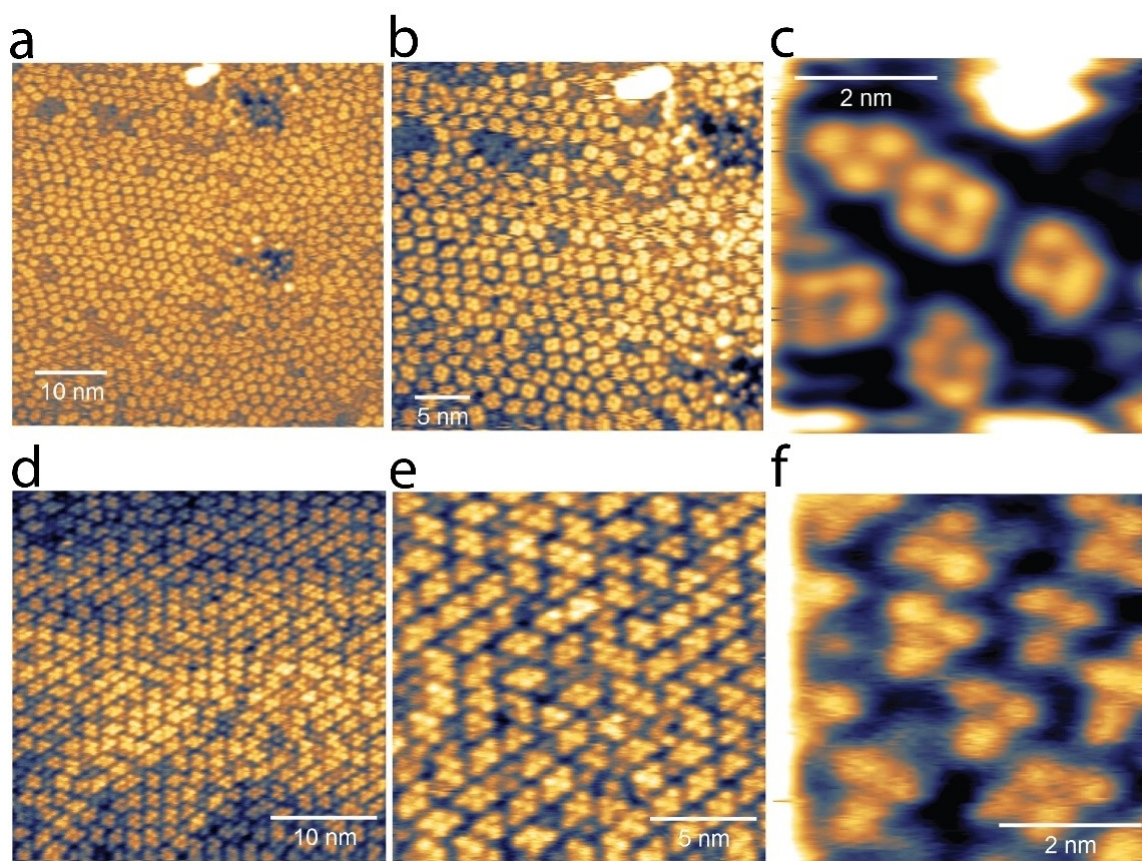


**Figure 5.** a–b. STM images of NHO-1 on Au(111) (130 K, +1.3 V, 0.2 nA). c. High resolution STM image of trimers and tetramers of NHO-1 (130 K, +1.6 V, 0.25 nA). d–e. STM images of NHO-2 on Au(111) (130 K, +1.3 V, 0.2 nA). f. High resolution STM image of trimers and tetramers of NHO-2 (130 K, +1.0 V, 0.2 nA).

correlated to physisorbed species that limited the formation of a high surface density monolayer. In the case of NHO-1, tetramers equally formed a square or a rhombic shape (Figure 5c), while tetramers were mostly detected in stretched rhombic shape for NHO-2 (Figure 5f).

DFT simulations were conducted to elucidate the self-assembly patterns of NHOs. The adsorption patterns of NHO-2-Au-adatom complexes for the formation of coupled dimers (Figure 6a), trimers (Figure 6b) and tetramers (Figure 6c) were simulated and fit well the experimental STM images (Figures 6d–6f). The simulations were performed for NHO-2, and very similar patterns are expected for NHO-1, according to the resemblance of energetics, as listed in Table S1.

The calculations show that two, three and four NHO–Au-adatom complexes can self-assemble while gaining 0.07–0.08 eV/molecule in forming dimers, trimers, or tetramers with Au-adatom per NHO (see models in Figure S26). Conversely, the adsorption of a second NHO-2 molecule on the same Au-adatom is less favorable, by 0.78 eV, with respect to adsorption on a separate adatom in a dimer. While the closely squared tetramers can be attributed to four NHO–Au complexes (Figure 6c and 6f), the stretched rhombic tetramers better fit the two dimers scenario (Figure 6a and 6d). In fact, the latter configuration

is also stable, although with a lower energy gain of 0.02 eV/molecule with respect to isolated NHO–Au-adatom complexes (see Table S1). The observation that stretched tetramers are mostly observed in large scale images (Figure 5d and 5e), may be attributed to activation barriers in fusing two dimers or to intermolecular interactions among adjacent supramolecular complexes that are neglected in present calculations. The absence of peripheral methyl groups in NHO-1 supramolecular complexes, as well as the overall lower surface density, favors a larger mobility, hence explaining the larger variety of tetrameric aggregates.

It was previously demonstrated that <sup>Me</sup>NHC molecules are self-assembled on Au surface and form dimers and trimers that are linked via a single Au-adatom.<sup>[11c]</sup> This assembly pattern is different than the self-assembly of NHOs that involve the assembly of NHO–Au-adatom complexes, in which each NHO is coordinated to Au-adatom.<sup>[11c,d]</sup> This distinct self-assembly pattern of NHOs is correlated to strong NHO–Au interactions and steric hindrance between adsorbates that lead to adsorption geometries that prevent the assembly of two NHO molecules on a single Au-adatom.

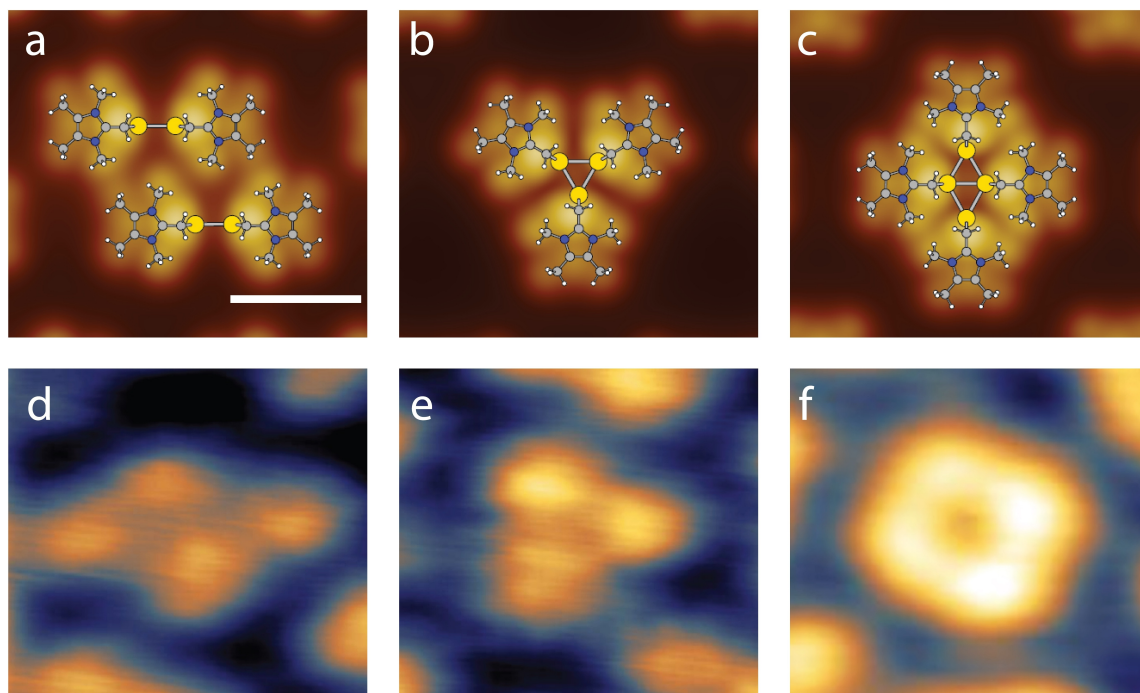


**Figure 6.** Simulated STM images of (a) pair of dimers, (b) trimers, and (c) tetramers of NHO-2-Au-adatom complexes and corresponding STM images of NHO-2 (d and e) and NHO-1 (f). Scale bar equals 1 nm.

## Conclusion

In this work we demonstrate that NHOs form thermally stable, chemisorbed monolayers on Au(111). The monolayers were characterized with improved thermal stability, and larger effect on the work function that, for methyl-functionalized NHO-2, surpass that of <sup>Me</sup>NHC. NHOs were found to adsorb in a flat-lying adsorption geometry on a Au-adatom via end-on carbon coordination. At room temperature, the molecules were self-assembled in dimers, trimers and tetramers, constructed of two, three, and four NHO–Au-adatom complexes, respectively. The improved thermal stability of NHOs on Au(111) and their impact on work function properties demonstrate the crucial role of the surface-anchoring CH<sub>2</sub>-group on the molecular flexibility that yielded optimized adsorption geometry. The molecular flexibility enabled to utilize NHO backbone functionalization to further improve the thermal stability and the impact on work function. By analyzing the surface properties of NHO monolayers, this work demonstrates the critical role of the surface-anchoring carbon species and its impact in tuning the surface properties of self-assembled monolayers.

## Acknowledgements

This research was supported by the European Research Council (ERC) under the European Union's Horizon 2020 and Horizon Europe research and innovation program (Grant Agreement No. 802769, ERC Starting Grant “Map-Cat” and Grant Agreement No. 101077332, ERC Starting Grant “CC-CHARGED”). I. B. acknowledges the Cloro

Israel Foundation, and the Harvey M. Krueger Family Center for Nanoscience and Nanotechnology for their financial support. L.L. acknowledges Harvey M. Krueger Family Center for Nanoscience and Nanotechnology for their financial support. This project has received funding from the European Union's Horizon 2020 and Horizon Europe research and innovation program under grant agreement No. 101007417 and 101077332 having benefited from the access to OSMOS STM lab provided by CNR-IOM in Trieste and by the Physics Department of the University of Milan for theoretical support, within the framework of the NFFA-Europe Pilot Transnational Access Activity, proposal ID443. We acknowledge the CINECA award under the ISCRA initiative, for the availability of high performance computing resources and support.

## Conflict of Interest

The authors declare no conflict of interest.

## Data Availability Statement

The data that support the findings of this study are available from the corresponding author upon reasonable request.

**Keywords:** N-Heterocyclic Olefins · Scanning Tunneling Microscopy · Self-Assembled Monolayers · Surface Chemistry · X-Ray Absorption Spectroscopy

- [1] a) A. V. Zhukhovitskiy, M. J. MacLeod, J. A. Johnson, *Chem. Rev.* **2015**, *115*, 11503–11532; b) C. A. Smith, M. R. Narouz, P. A. Lummis, I. Singh, A. Nazemi, C. H. Li, C. M. Crudden, *Chem. Rev.* **2019**, *119*, 4986–5056; c) M. Koy, P. Bellotti, M. Das, F. Glorius, *Nat. Catal.* **2021**, *4*, 352–363; d) G. Kaur, R. L. Thimes, J. P. Camden, D. M. Jenkins, *Chem. Commun.* **2022**, *58*, 13188–13197; e) H. Shen, G. L. Tian, Z. Xu, L. Z. Wang, Q. Y. Wu, Y. H. Zhang, B. K. Teo, N. F. Zheng, *Coord. Chem. Rev.* **2022**, *458*, 214425; f) J. J. Navarro, M. Das, S. Tosoni, F. Landwehr, J. P. Bruce, M. Heyde, G. Pacchioni, B. Roland Cuenya, F. Glorius, *J. Am. Chem. Soc.* **2022**, *144*, 16267–16271.
- [2] a) C. M. Crudden, J. H. Horton, I. I. Ebralidze, O. V. Zenkina, A. B. McLean, B. Drevniok, Z. She, H. B. Kraatz, N. J. Mosey, T. Seki, E. C. Keske, J. D. Leake, A. Rousina-Webb, G. Wu, *Nat. Chem.* **2014**, *6*, 409–414; b) D. T. Nguyen, M. Freitag, M. Korsgen, S. Lamping, A. Ruhling, A. H. Schafer, M. H. Siekman, H. F. Arlinghaus, W. G. van der Wiel, F. Glorius, B. J. Ravoo, *Angew. Chem. Int. Ed.* **2018**, *57*, 11465–11469; c) J. F. DeJesus, L. M. Sherman, D. J. Yohannan, J. C. Becca, S. L. Strausser, L. F. P. Karger, L. Jensen, D. M. Jenkins, J. P. Camden, *Angew. Chem. Int. Ed.* **2020**, *59*, 7585–7590.
- [3] a) A. Ferry, K. Schaepe, P. Tegeger, C. Richter, K. M. Chepiga, B. J. Ravoo, F. Glorius, *ACS Catal.* **2015**, *5*, 5414–5420; b) C. M. Crudden, J. H. Horton, M. R. Narouz, Z. J. Li, C. A. Smith, K. Munro, C. J. Baddeley, C. R. Larrea, B. Drevniok, B. Thanabalasingam, A. B. McLean, O. V. Zenkina, I. I. Ebralidze, Z. She, H. B. Kraatz, N. J. Mosey, L. N. Saunders, A. Yagi, *Nat. Commun.* **2016**, *7*, 12654; c) A. V. Zhukhovitskiy, M. G. Mavros, K. T. Queeney, T. Wu, T. Van Voorhis, J. A. Johnson, *J. Am. Chem. Soc.* **2016**, *138*, 8639–8652; d) S. Dery, S. Kim, G. Tomaschun, D. Haddad, A. Cossaro, A. Verdini, L. Floreano, T. Kluner, F. D. Toste, E. Gross, *Chem. Eur. J.* **2019**, *25*, 15067–15072; e) S. Dery, S. Kim, G. Tomaschun, I. Berg, D. Feferman, A. Cossaro, A. Verdini, L. Floreano, T. Kluner, F. D. Toste, E. Gross, *J. Phys. Chem. Lett.* **2019**, *10*, 5099–5104; f) M. J. MacLeod, A. J. Goodman, H. Z. Ye, H. V. T. Nguyen, T. Van Voorhis, J. A. Johnson, *Nat. Chem.* **2019**, *11*, 57–63; g) D. T. Nguyen, M. Freitag, C. Gutheil, K. Sotthewes, B. J. Tyler, M. Bockmann, M. Das, F. Schluter, N. L. Doltsinis, H. F. Arlinghaus, B. J. Ravoo, F. Glorius, *Angew. Chem. Int. Ed.* **2020**, *59*, 13651–13656; h) E. Amit, L. Dery, S. Dery, S. Kim, A. Roy, Q. C. Hu, V. Gutkin, H. Eisenberg, T. Stein, D. Mandler, F. D. Toste, E. Gross, *Nat. Commun.* **2020**, *11*, 5714; i) S. Dery, I. Berg, S. Kim, A. Cossaro, A. Verdini, L. Floreano, F. D. Toste, E. Gross, *Langmuir* **2020**, *36*, 697–703; j) I. Berg, L. Hale, M. Carmiel-Kostan, F. D. Toste, E. Gross, *Chem. Commun.* **2021**, *57*, 5342–5345; k) S. Dery, I. Alshanski, E. Mervinetsky, D. Feferman, S. Yitzchaik, M. Hurevich, E. Gross, *Chem. Commun.* **2021**, *57*, 6233–6236; l) S. Dery, P. Bellotti, T. Ben-Tzvi, M. Freitag, T. Shahar, A. Cossaro, A. Verdini, L. Floreano, F. Glorius, E. Gross, *Langmuir* **2021**, *37*, 10029–10035; m) P. Bellotti, M. Koy, M. N. Hopkinson, F. Glorius, *Nat. Chem. Rev.* **2021**, *5*, 711–725.
- [4] a) Z. J. Li, M. R. Narouz, K. Munro, B. Hao, C. M. Crudden, J. H. Horton, H. X. Hao, *ACS Appl. Mater. Interfaces* **2017**, *9*, 39223–39234; b) S. R. Thomas, A. Casini, *J. Organomet. Chem.* **2021**, *938*, 121743.
- [5] a) C. Richter, K. Schaepe, F. Glorius, B. J. Ravoo, *Chem. Commun.* **2014**, *50*, 3204–3207; b) M. J. MacLeod, J. A. Johnson, *J. Am. Chem. Soc.* **2015**, *137*, 7974–7977; c) H. P. Lu, Z. H. Zhou, O. V. Prezhdo, R. L. Brutchey, *J. Am. Chem. Soc.* **2016**, *138*, 14844–14847; d) K. Salorinne, R. W. Y. Man, C. H. Li, M. Taki, M. Nambo, C. M. Crudden, *Angew. Chem. Int. Ed.* **2017**, *56*, 6198–6202; e) L. M. Martinez-Prieto, L. Rakers, A. M. Lopez-Vinasco, I. Cano, Y. Coppel, K. Philippot, F. Glorius, B. Chaudret, P. W. N. M. van Leeuwen, *Chem. Eur. J.* **2017**, *23*, 12779–12786; f) H. P. Lu, R. L. Brutchey, *Chem. Mater.* **2017**, *29*, 1396–1403; g) M. R. Narouz, K. M. Osten, P. J. Unsworth, R. W. Y. Man, K. Salorinne, S. Takano, R. Tomihara, S. Kaappa, S. Malola, C. T. Dinh, J. D. Padmos, K. Ayoo, P. J. Garrett, M. Nambo, J. H. Horton, E. H. Sargent, H. Hakkinen, T. Tsukuda, C. M. Crudden, *Nat. Chem.* **2019**, *11*, 419–425; h) N. Kaeffer, D. Mance, C. Coperet, *Angew. Chem. Int. Ed.* **2020**, *59*, 19999–20007; i) D. E. Westmoreland, R. Lopez-Arteaga, E. A. Weiss, *J. Am. Chem. Soc.* **2020**, *142*, 2690–2696; j) H. Shen, Q. Y. Wu, S. Malola, Y. Z. Han, Z. Xu, R. X. Qin, X. K. Tang, Y. B. Chen, B. K. Teo, H. Hakkinen, N. F. Zheng, *J. Am. Chem. Soc.* **2022**, *144*, 10844–10853.
- [6] a) Y. Levratovsky, E. Gross, *Faraday Discuss.* **2016**, *188*, 345–353; b) C. Y. Wu, W. J. Wolf, Y. Levartovsky, H. A. Bechtel, M. C. Martin, F. D. Toste, E. Gross, *Nature* **2017**, *541*, 511–515; c) S. Dery, E. Amit, E. Gross, *Top. Catal.* **2018**, *61*, 923–939; d) S. Dery, S. Kim, D. Haddad, A. Cossaro, A. Verdini, L. Floreano, F. D. Toste, E. Gross, *Chem. Sci.* **2018**, *9*, 6523–6531; e) S. Dery, S. Kim, D. Feferman, H. Mehlman, F. D. Toste, E. Gross, *Phys. Chem. Chem. Phys.* **2020**, *22*, 18765–18769; f) L. Rikanati, S. Dery, E. Gross, *J. Chem. Phys.* **2021**, *155*, 204704; g) S. Dery, H. Mehlman, L. Hale, M. Carmiel-Kostan, R. Yemini, T. Ben-Tzvi, M. Noked, F. D. Toste, E. Gross, *ACS Catal.* **2021**, *11*, 9875–9884.
- [7] a) H. K. Kim, A. S. Hyla, P. Winget, H. Li, C. M. Wyss, A. J. Jordan, F. A. Larrain, J. P. Sadighi, C. Fuentes-Hernandez, B. Kippelen, J. L. Bredas, S. Barlow, S. R. Marder, *Chem. Mater.* **2017**, *29*, 3403–3411; b) A. F. Lv, M. Freitag, K. M. Chepiga, A. H. Schafer, F. Glorius, L. F. Chi, *Angew. Chem. Int. Ed.* **2018**, *57*, 4792–4796; c) S. Kang, S. Park, H. Kang, S. J. Cho, H. Song, H. J. Yoon, *Chem. Commun.* **2019**, *55*, 8780–8783; d) Z. F. Wang, M. Das, C. Gutheil, H. Osthuus, F. Strieth-Kalthoff, A. Timmer, N. L. Doltsinis, W. C. Wang, L. F. Chi, F. Glorius, *J. Mater. Chem. C* **2022**, *10*, 8589–8595.
- [8] I. Berg, E. Amit, L. Hale, F. D. Toste, E. Gross, *Angew. Chem. Int. Ed.* **2022**, *61*, e202201093.
- [9] a) K. V. S. Ranganath, J. Kloesges, A. H. Schafer, F. Glorius, *Angew. Chem. Int. Ed.* **2010**, *49*, 7786–7789; b) P. Lara, A. Suarez, V. Colliere, K. Philippot, B. Chaudret, *ChemCatChem* **2014**, *6*, 87–90; c) R. Ye, A. V. Zhukhovitskiy, R. V. Kazantsev, S. C. Fakra, B. B. Wickemeyer, F. D. Toste, G. A. Somorjai, *J. Am. Chem. Soc.* **2018**, *140*, 4144–4149; d) P. Tegeger, M. Freitag, K. M. Chepiga, S. Muratsugu, N. Moller, S. Lamping, M. Tada, F. Glorius, B. J. Ravoo, *Chem. Eur. J.* **2018**, *24*, 18682–18688; e) L. Stephens, J. D. Padmos, M. R. Narouz, A. Al-Rashed, C. H. Li, N. Payne, M. Zamora, C. M. Crudden, J. Mauzeroll, J. H. Horton, *J. Electrochem. Soc.* **2018**, *165*, G139–G145; f) N. Kaeffer, H. J. Liu, H. K. Lo, A. Fedorov, C. Coperet, *Chem. Sci.* **2018**, *9*, 5366–5371; g) X. X. Gou, T. Liu, Y. Y. Wang, Y. F. Han, *Angew. Chem. Int. Ed.* **2020**, *59*, 16683–16689.
- [10] a) T. Droge, F. Glorius, *Angew. Chem. Int. Ed.* **2010**, *49*, 6940–6952; b) D. J. Nelson, S. P. Nolan, *Chem. Soc. Rev.* **2013**, *42*, 6723–6753; c) H. V. Huynh, *Chem. Rev.* **2018**, *118*, 9457–9492.
- [11] a) A. V. Zhukhovitskiy, M. G. Mavros, T. Van Voorhis, J. A. Johnson, *J. Am. Chem. Soc.* **2013**, *135*, 7418–7421; b) C. R. Larrea, C. J. Baddeley, M. R. Narouz, N. J. Mosey, J. H. Horton, C. M. Crudden, *ChemPhysChem* **2017**, *18*, 3536–3539; c) G. Q. Wang, A. Ruhling, S. Amirjalayer, M. Knor, J. B. Ernst, C. Richter, H. J. Gao, A. Timmer, H. Y. Gao, N. L. Doltsinis, F. Glorius, H. Fuchs, *Nat. Chem.* **2017**, *9*, 152–156; d) A. Bakker, A. Timmer, E. Kolodzeiski, M. Freitag, H. Y. Gao, H. Monig, S. Amirjalayer, F. Glorius, H. Fuchs, *J. Am. Chem. Soc.* **2018**, *140*, 11889–11892.

- [12] a) V. Lavallo, Y. Canac, C. Prasang, B. Donnadiu, G. Bertrand, *Angew. Chem. Int. Ed.* **2005**, *44*, 5705–5709; b) A. Bakker, M. Freitag, E. Kolodzeiski, P. Bellotti, A. Timmer, J. D. Ren, B. S. Lammers, D. Moock, H. W. Roesky, H. Monig, S. Amirjalayer, H. Fuchs, F. Glorius, *Angew. Chem. Int. Ed.* **2020**, *59*, 13643–13646.
- [13] D. T. H. Nguyen, L. R. Shultz, T. Jurca, A. Nazemi, *Langmuir* **2023**, *39*, 3204–3215.
- [14] E. Amit, I. Berg, E. Gross, *Chem. Eur. J.* **2020**, *26*, 13046–13052.
- [15] M. M. D. Roy, E. Rivard, *Acc. Chem. Res.* **2017**, *50*, 2017–2025.
- [16] a) N. Kuhn, H. Bohnen, J. Kreuzberg, D. Blaser, R. Boese, *J. Chem. Soc. Chem. Commun.* **1993**, 1136–1137; b) M. M. Hansmann, P. W. Antoni, H. Pesch, *Angew. Chem. Int. Ed.* **2020**, *59*, 5782–5787.
- [17] S. M. I. Al-Rafia, A. C. Malcolm, S. K. Liew, M. J. Ferguson, R. McDonald, E. Rivard, *Chem. Commun.* **2011**, *47*, 6987–6989.
- [18] S. Naumann, *Chem. Commun.* **2019**, *55*, 11658–11670.
- [19] a) A. Furstner, M. Alcarazo, R. Goddard, C. W. Lehmann, *Angew. Chem. Int. Ed.* **2008**, *47*, 3210–3214; b) B. Maji, M. Horn, H. Mayr, *Angew. Chem. Int. Ed.* **2012**, *51*, 6231–6235; c) K. Powers, C. Hering-Junghans, R. McDonald, M. J. Ferguson, E. Rivard, *Polyhedron* **2016**, *108*, 8–14.
- [20] a) A. Dumrath, X. F. Wu, H. Neumann, A. Spannenberg, R. Jackstell, M. Beller, *Angew. Chem. Int. Ed.* **2010**, *49*, 8988–8992; b) Y. B. Wang, Y. M. Wang, W. Z. Zhang, X. B. Lu, *J. Am. Chem. Soc.* **2013**, *135*, 11996–12003; c) M. Blumel, R. D. Crocker, J. B. Harper, D. Enders, T. V. Nguyen, *Chem. Commun.* **2016**, *52*, 7958–7961; d) W. Y. Li, N. Yang, Y. J. Lyu, *J. Org. Chem.* **2016**, *81*, 5303–5313; e) V. B. Saptal, B. M. Bhanage, *ChemSusChem* **2016**, *9*, 1980–1985; f) U. Kaya, U. P. N. Tran, D. Enders, J. Ho, T. V. Nguyen, *Org. Lett.* **2017**, *19*, 1398–1401; g) A. Schumann, C. Hering-Junghans, *Eur. J. Inorg. Chem.* **2018**, 2584–2588; h) I. C. Watson, A. Schumann, H. Y. Yu, E. C. Davy, R. McDonald, M. J. Ferguson, C. Hering-Junghans, E. Rivard, *Chem. Eur. J.* **2019**, *25*, 9678–9690.
- [21] a) S. M. I. Al-Rafia, M. J. Ferguson, E. Rivard, *Inorg. Chem.* **2011**, *50*, 10543–10545; b) Y. Z. Wang, M. Y. Abraham, R. J. Gilliard, D. R. Sexton, P. R. Wei, G. H. Robinson, *Organometallics* **2013**, *32*, 6639–6642; c) R. S. Ghadwal, S. O. Reichmann, F. Engelhardt, D. M. Andrada, G. Frenking, *Chem. Commun.* **2013**, *49*, 9440–9442; d) S. M. I. Al-Rafia, M. R. Momeni, R. McDonald, M. J. Ferguson, A. Brown, E. Rivard, *Angew. Chem. Int. Ed.* **2013**, *52*, 6390–6395; e) K. Schwedtmann, R. Schoemaker, F. Hengersdorf, A. Bauza, A. Frontera, R. Weiss, J. J. Weigand, *Dalton Trans.* **2016**, *45*, 11384–11396; f) A. Casero, H. Elsen, J. Pahl, S. Harder, *Angew. Chem. Int. Ed.* **2017**, *56*, 6906–6910; g) C. Hering-Junghans, P. Andreiuk, M. J. Ferguson, R. McDonald, E. Rivard, *Angew. Chem. Int. Ed.* **2017**, *56*, 6272–6275; h) A. P. D. Batista, A. G. S. de Oliveira-Filho, S. E. Galembek, *ACS Omega* **2017**, *2*, 299–307; i) T. X. Gentner, G. Ballmann, J. Pahl, H. Eisen, S. Harder, *Organometallics* **2018**, *37*, 4473–4480.
- [22] a) P. P. Ponti, J. C. Baldwin, W. C. Kaska, *Inorg. Chem.* **1979**, *18*, 873–875; b) M. Viciano, M. Feliz, R. Corberan, J. A. Mata, E. Clot, E. Peris, *Organometallics* **2007**, *26*, 5304–5314; c) G. Y. Song, X. W. Li, Z. C. Song, J. Zhao, H. J. Zhang, *Chem. Eur. J.* **2009**, *15*, 5535–5544; d) A. Iturmendi, N. Garcia, E. A. Jaseer, J. Munarriz, P. J. S. Miguel, V. Polo, M. Iglesias, L. A. Oro, *Dalton Trans.* **2016**, *45*, 12835–12845.
- [23] a) S. Naumann, A. W. Thomas, A. P. Dove, *Angew. Chem. Int. Ed.* **2015**, *54*, 9550–9554; b) H. Y. Wang, Q. Y. Wang, J. H. He, Y. T. Zhang, *Polym. Chem.* **2019**, *10*, 3597–3603; c) P. Walther, A. Krauss, S. Naumann, *Angew. Chem. Int. Ed.* **2019**, *58*, 10737–10741.
- [24] a) M. B. Gildner, T. W. Hudnall, *Chem. Commun.* **2019**, *55*, 12300–12303; b) G. R. Meng, L. Kakalis, S. P. Nolan, M. Szostak, *Tetrahedron Lett.* **2019**, *60*, 378–381; c) L. M. Sherman, S. L. Strausser, R. K. Borsari, D. M. Jenkins, J. P. Camden, *Langmuir* **2021**, *37*, 5864–5871.
- [25] a) M. J. Trujillo, S. L. Strausser, J. C. Becca, J. F. DeJesus, L. Jensen, D. M. Jenkins, J. P. Camden, *J. Phys. Chem. Lett.* **2018**, *9*, 6779–6785; b) J. F. DeJesus, M. J. Trujillo, J. P. Camden, D. M. Jenkins, *J. Am. Chem. Soc.* **2018**, *140*, 1247–1250; c) G. Lovat, E. A. Doud, D. Y. Lu, G. Kladnik, M. S. Inkpen, M. L. Steigerwald, D. Cvetko, M. S. Hybertsen, A. Morgante, X. Roy, L. Venkataraman, *Chem. Sci.* **2019**, *10*, 930–935.
- [26] a) L. Floreano, A. Cossaro, R. Gotter, A. Verdini, G. Bavdek, F. Evangelista, A. Ruocco, A. Morgante, D. Cvetko, *J. Phys. Chem. C* **2008**, *112*, 10794–10802; b) A. Calabrese, L. Floreano, A. Verdini, C. Mariani, M. G. Betti, *Phys. Rev. B* **2009**, *79*, 115446.
- [27] M. R. Narouz, C. H. Li, A. Nazemi, C. M. Crudden, *Langmuir* **2017**, *33*, 14211–14219.
- [28] X. P. Cao, R. J. Hamers, *J. Am. Chem. Soc.* **2001**, *123*, 10988–10996.
- [29] N. Graf, E. Yegen, T. Gross, A. Lippitz, W. Weigel, S. Krakert, A. Terfort, W. E. S. Unger, *Surf. Sci.* **2009**, *603*, 2849–2860.
- [30] a) S. Rangan, F. Bournel, J. J. Gallet, S. Kubsy, K. Le Guen, G. Dufour, F. Rochet, F. Sirotti, S. Carniato, V. Ilakovac, *Phys. Rev. B* **2005**, *71*, 165319; b) V. Ilakovac, S. Carniato, J. J. Gallet, E. Kukk, D. Horvatic, A. Ilakovac, *Phys. Rev. A* **2008**, *77*, 012516; c) H. Min, P. L. Girard-Lauriault, T. Gross, A. Lippitz, P. Dietrich, W. E. S. Unger, *Anal. Bioanal. Chem.* **2012**, *403*, 613–623.
- [31] Y. H. La, Y. J. Jung, T. H. Kang, K. Ihm, K. J. Kim, B. Kim, J. W. Park, *Langmuir* **2003**, *19*, 9984–9987.
- [32] M. Jain, U. Gerstmann, W. G. Schmidt, H. Aldahhak, *J. Comput. Chem.* **2022**, *43*, 413–420.
- [33] A. Ravikumar, A. Baby, H. Lin, G. P. Brivio, G. Fratesi, *Sci. Rep.* **2016**, *6*, 24603.
- [34] R. J. J. Jansen, H. Vanbekkum, *Carbon* **1995**, *33*, 1021–1027.

Manuscript received: August 14, 2023

Accepted manuscript online: September 24, 2023

Version of record online: October 11, 2023